

# Quantum to classical transition via fuzzy measurements on high gain spontaneous parametric down-conversion

Chiara Vitelli,<sup>1,2</sup> Nicolò Spagnolo,<sup>1,2</sup> Lorenzo Toffoli,<sup>1</sup> Fabio Sciarrino,<sup>1,3</sup> and Francesco De Martini<sup>1,4</sup>

<sup>1</sup>*Dipartimento di Fisica, “Sapienza” Università di Roma, piazzale Aldo Moro 5, I-00185 Roma, Italy*

<sup>2</sup>*Consorzio Nazionale Interuniversitario per le Scienze Fisiche della Materia, piazzale Aldo Moro 5, I-00185 Roma, Italy*

<sup>3</sup>*Istituto Nazionale di Ottica Applicata, largo Fermi 6, I-50125 Firenze, Italy*

<sup>4</sup>*Accademia Nazionale dei Lincei, via della Lungara 10, I-00165 Roma, Italy*

We consider the high gain spontaneous parametric down-conversion in a non collinear geometry as a paradigmatic scenario to investigate the quantum-to-classical transition by increasing the pump power, that is, the average number of generated photons. The possibility of observing quantum correlations in such macroscopic quantum system through dichotomic measurement will be analyzed by addressing two different measurement schemes, based on different dichotomization processes. More specifically, we will investigate the persistence of non-locality in an increasing size  $\frac{n}{2}$ -spin singlet state by studying the change in the correlations form as  $n$  increases, both in the ideal case and in presence of losses. We observe a fast decrease in the amount of Bell’s inequality violation for increasing system size. This theoretical analysis is supported by the experimental observation of macro-macro correlations with an average number of photons of about  $10^3$ . Our results enlighten the practical extreme difficulty of observing non-locality by performing such a dichotomic fuzzy measurement.

PACS numbers:

## I. INTRODUCTION

For long time the investigation about entanglement and non-locality has been limited to quantum systems of small size [1]. Theoretical and experimental works on Bell’s inequalities have been devoted to the study of single particle states, in which dichotomic measurements have been performed [2]. Non-locality tests have been achieved with single photon states, produced by parametric down conversion, by detecting polarization correlations [3–5]. More recently the violation of Bell’s inequality has been performed with a larger number of photons: on GHZ [6] and cluster states [7] up to 4 photons. On the other hand, the possibility of observing quantum phenomena at a macroscopic level seems to be in conflict with the classical description of our everyday world knowledge. The main problem for such observation arises from the experimental difficulty of sufficiently isolating a quantum system from its environment, i.e., from the decoherence process [8]. An alternative approach to explain the quantum-to-classical transition, conceptually different from the decoherence program, has been given, very recently, by Kofler and Brukner, along the idea earlier discussed by Bell, Peres [9] and others. They have given a description of the emergence of macroscopic realism and classical physics in systems of increasing size *within quantum theory* [10]. They focused on the limits of the quantum effects observability in macroscopic objects, showing that, for large systems, macrorealism arises under coarse-grained measurements. More specifically they demonstrated that, while the evolution of a large spin cannot be described classically when sharp measurement are performed, a fuzzy measurement on a large spin system would induce the emergence of the Newtonian time evolution from a full quantum description of the spin

state. However, some counterexamples to such modelization have been found later by the same authors: some non classical Hamiltonians violate macrorealism despite coarse-grained measurements [11]. One example is given by the time-dependent Schrödinger catlike superposition, which can violate macrorealism by adopting a suitable “which emisphere” measurement. Therefore the measurement problem seems to be a key ingredient in the attempt of understanding the limits of the quantum behavior of physical systems and the quantum-to-classical transition question. As a further step, Kofler, Bruic and Brukner also demonstrated [12] that macrorealism does not imply a continuous spatiotemporal evolution. Indeed, they showed that the same Schrödinger catlike non-classical Hamiltonian, in contact with a dephasing environment does not violate any longer a Leggett-Garg inequality, while it still presents a non-classical time evolution. In a recent paper Jeong et al. [13] contributed to the investigation about the possibility of observing the quantum features of a system when fuzzy measurement are performed on it, finding that extremely-coarse-grained measurements can still be useful to reveal the quantum world where local realism fails.

In this context, the possibility of obtaining macroscopic quantum systems in laboratory has raised the problem of investigating entanglement and non locality in systems in which single particles cannot be addressed singularly. As shown in Ref. [14], the demonstration of non-locality in a multiphoton state produced by a non-degenerate optical parametric amplifier would require the experimental application of parity operators. On the other hand, the estimation of a coarse grained quantity, through collective measurements as the ones proposed in Ref. [15], would miss the underlying quantum structure of the generated state, introducing elements of local re-

alism even in presence of strong entanglement and in absence of decoherence. The theoretical investigation on a multiphoton system, obtained via parametric down conversion, has been also carried out by Reid et al. [16]. They analyzed the possibility of obtaining the violation of Bell's inequality by performing dichotomic measurement on the multiparticle quantum state. More specifically, in analogy with the spin formalism, they proposed to compare the number of photons polarized "up" with the number of photons polarized "down" at the exit of the amplifier. The result of this comparison could be either (+1) or (-1) hence the measurement on the multiphoton state turned out to be dichotomic. In such a way Reid et al. revealed a small violation of the multiparticle Bell's inequality even in presence of losses and quantum inefficiency of detectors. It's worth noting that this violation presents a fast decreasing behavior as a function of the generated photons number. In a recent paper, Bancal et al. [17] have discussed different techniques for testing Bell's inequalities in multipair scenarios, in which either at Alice's and Bob's site a global measurement is performed. They distinguished between two cases: distinguishable, i.e. independent, and indistinguishable, i.e. belonging to the same spatial and temporal mode, photon pairs. They found that while the state of indistinguishable pairs results more entangled, the state of independent pairs appears to be more nonlocal.

In the present manuscript, we investigate the macroscopic-macroscopic state generated by high gain spontaneous parametric down-conversion. The possibility of observing quantum correlations in macroscopic quantum systems through dichotomic measurement will be analyzed, by addressing two different measurement schemes, based on different dichotomization processes. More specifically, we will investigate the persistence of non-locality in an increasing size  $\frac{n}{2}$ -spin singlet state by studying the change in the correlations form as  $n$  increases, both in the ideal case and in presence of losses. At last, experimental observation of macro-macro correlations will be reported. The results obtained enlighten that dichotomic fuzzy measurements lack of the necessary resolution to characterize such states and show the extreme difficulty to observe quantum non-locality in this experimental configuration.

Let us give a brief outline of the paper. Section II is devoted to the introduction of the analyzed quantum system. In Section III, we describe two different types of dichotomic measurements on multiphoton states: the orthogonality filtering (OF) and the threshold detection (TD). In Section IV we present the results of the numerical simulations of the correlations between dichotomic measurements carried out on the multiphoton fields produced via spontaneous parametric down conversion. We report the theoretical interference fringe-patterns for single- $\frac{n}{2}$  states, we observe a transition from the sinusoidal pattern of the spin- $\frac{1}{2}$  into a quasi-linear pattern by increasing the number of photons of the spin state. According to this behavior we observe a progres-

sive decrease in the amount of the violation as also predicted in Ref [16, 17]. As following step, we estimate the correlation after propagation over a lossy channel. We then analyze the response of the system to the two dichotomic measurements reported in Sec.III, discussing the feasibility of a CHSH test with these detection strategies. Finally, Section V is dedicated to an experimental test of the previous results.

## II. MACROSCOPIC QUANTUM STATE BASED ON HIGH GAIN SPONTANEOUS PARAMETRIC DOWN-CONVERSION

The investigation on the micro-macro transition will be performed on a paradigmatic physical system: the optical parametric amplifier working in a high gain regime. The quantum state produced in a low gain regime has been experimentally realized and deeply studied in the past few years [19, 20]. We are now interested in analyzing the behavior of such quantum system when the number of photons is increased and it undergoes a fuzzy measurement, in which the generated particles cannot be addressed singularly, but a dichotomic measurement is performed on the overall state. More specifically, the radiation field under investigation is the quantum state obtained by spontaneous parametric down-conversion (SPDC) with an EPR type-II source [19, 21], whose interaction Hamiltonian is:  $\mathcal{H}_{int} = i\hbar\chi \left( \hat{a}_\pi^\dagger \hat{b}_{\pi\perp}^\dagger - \hat{a}_{\pi\perp}^\dagger \hat{b}_\pi^\dagger \right) + \text{H.c.}$  where  $\hat{a}_\pi^\dagger$  and  $\hat{b}_\pi^\dagger$  are the creation operators corresponding to the generation of a  $\pi$ -polarized photon on spatial modes  $\mathbf{k}_A$  and  $\mathbf{k}_B$ , as sketched in Fig.1, and  $\chi$  is the constant describing the strength of the interaction. The adoption of the single mode interaction Hamiltonian  $\mathcal{H}_{int}$  to model the SPDC source is valid since in our experimental setup, described in Sec.V, spatial and spectral filtering are performed on the generated field. A detailed analysis of the model taking into account a broadband pump pulse can be found in reference [22].

The output state reads [18–20]:

$$|\Psi^-\rangle = \frac{1}{C^2} \sum_{n=0}^{\infty} \Gamma^n \sqrt{n+1} |\psi_n^-\rangle \quad (1)$$

$$|\psi_n^-\rangle = \frac{1}{\sqrt{n+1}} \sum_{m=0}^n (-1)^m |(n-m)\pi, m\pi_\perp\rangle_A |m\pi, (n-m)\pi_\perp\rangle_B \quad (2)$$

where  $\Gamma = \tanh g$  and  $C = \cosh g$ ;  $g = \chi t$  is the nonlinear gain (NL) of the process. Hence, the output state can be written as the weighted coherent superposition of singlet spin- $\frac{n}{2}$  states  $|\psi_n^-\rangle$ .

As said, this EPR source has been already studied in different gain regimes. First, Kwiat et al. [21] exploited the polarization singlet-state emitted in the single-pair regime to obtain the violation of Bell's inequalities. Subsequent works studied the multi-photon states generated in a high gain SPDC source. Eibl. et al. [23] experimentally demonstrated four-photon entanglement in the

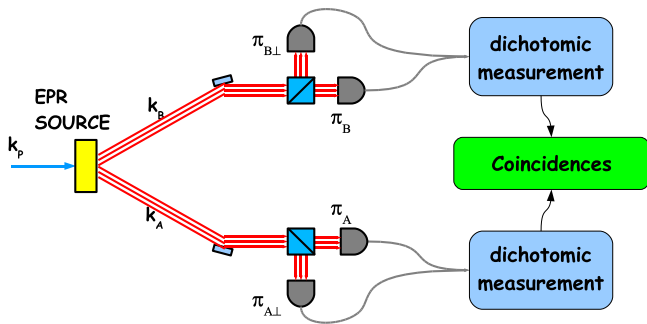


FIG. 1: (Color online) Scheme of the macroscopic-macroscopic source and of the detection apparatus. The multiphoton fields on the two spatial modes of an EPR source are analyzed in polarization with dichotomic measurements, where the +1 value is assigned if  $n_\pi > n_{\pi_\perp}$ , and -1 otherwise. Finally, coincidences between the two apparatuses are considered.

second-order emission state of the SPDC source, by taking the four-fold coincidences after the two output modes of the source were splitted by 50-50 beam-splitters. A generalized non-locality test [24] was also successfully performed in this configuration. A similar scheme was subsequently exploited by Wieczorek et al. [25] to experimentally generate an entire family of four-photon entangled states. The presence of polarization-entanglement in the multi-photon states up to 12 photons has been proved by studying the high losses regime where at most one photon per branch was detected [19]. The density matrix of this two-photons state was analytically derived and experimentally investigated in a more recent work [20], where it has been demonstrated that it coincides with the one of a Werner state (WS), i.e., a weighted superposition of a maximally entangled singlet state with a fully mixed state. Simon and Bouwmeester [18] derived a criteria to quantify the entanglement of the multiphoton states produced by a high gain SPDC source by measuring the Stokes parameters of polarization of the beams A and B. For a high efficiency detection observation of entanglement was predicted. However, no experimental demonstration of entanglement and non-locality has been given in the multi-photon regime where the generated state does not undergo to a controlled lossy detection scheme.

### III. DICHOTOMIC MEASUREMENTS ON MACROSCOPIC STATES

In the context of the investigation on entanglement and non-locality between macroscopic systems, Bell's inequalities have been generalized to many particle regimes. Among various strategies, several possible extensions of dichotomic measurements in the macroscopic regime have been presented [16, 17]. By these methods, CHSH-type inequalities can be exploited in order to perform

non-locality tests also in many-particle collective states.

In this section we analyze two possible kind of dichotomic measurements on macroscopic states, based on photon counting and signal processing techniques. The first technique is based on the Orthogonality-Filter (O-Filter) device [26, 27], which has already been used to test experimentally the entanglement between a microscopic and a macroscopic field. This method has several analogies with the detection strategy presented in Ref. [28] and attributed to a biological "human eye" detector. The second technique is a threshold dichotomic detection scheme, whose action is independent on the input state and hence can be fairly exploited for a Bell's inequalities test.

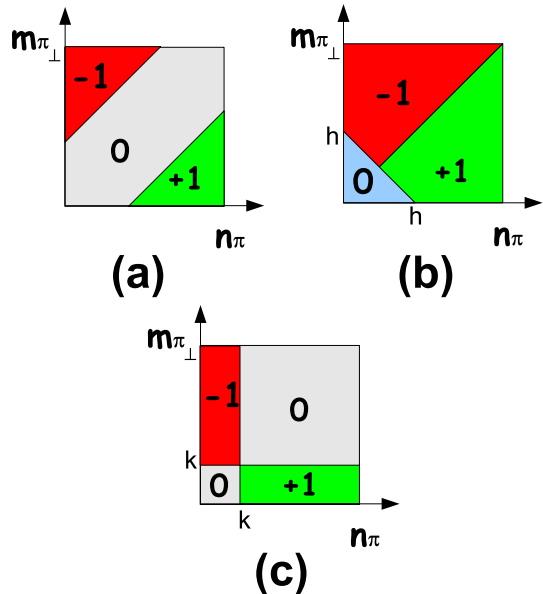


FIG. 2: (Color online) Selected regions of the Fock space for the two presented measurement schemes. Each diagram in this figure is referred to a single spatial mode. (a) O-Filtering technique representation in the bidimensional Fock-Space  $\{n_\pi, m_{\pi_\perp}\}$ . The (+1) and (-1) regions correspond to a difference in the detected photon numbers  $|n_\pi - m_{\pi_\perp}| > k$ . The (0) region corresponds to an inconclusive measurement. (b) Dichotomic threshold measurement representation in the bidimensional Fock-Space  $\{n_\pi, m_{\pi_\perp}\}$ . Only those pulses containing a sufficiently high photon number can be detected due to the threshold response of the apparatus. Then, a dichotomic assignment is performed on the measurement outcomes. (c) Response of "biological" detectors, which are sensible to the impinging field only if the photon number exceeds an intrinsic threshold  $k$ .

#### A. Orthogonality Filtering

The first dichotomic measurement technique we analyze in this section is based on the O-Filter (OF) device introduced in [26, 27]. In these papers the detection method allowed to discriminate among two macro-

scopic orthogonal states  $\{|\Phi^\phi\rangle, |\Phi^{\phi_\perp}\rangle\}$ , obtained by the collinear parametric amplification of single-photon states with equatorial polarization  $\{\vec{\pi}_\phi, \vec{\pi}_{\phi_\perp}\}$ , defined as  $\vec{\pi}_\phi = 2^{-1/2}(\vec{\pi}_H + e^{i\phi}\vec{\pi}_V)$ , by exploiting the difference in their photon number distributions. We utilize now this technique in a different experimental framework. Let us now give a formal description of this measurement technique in the POVM framework. First, the incident radiation is analyzed in polarization by a couple of photon-number resolving detectors on each spatial mode  $\{\mathbf{k}_A, \mathbf{k}_B\}$ . In the ideal case, this measurement corresponds to the projection of the impinging field onto the Von Neumann operators:  $\hat{\Pi}_{n,m} = |n\pi, m\pi_\perp\rangle\langle n\pi, m\pi_\perp|$ , where  $|n\pi, m\pi_\perp\rangle$  represents a quantum state with  $n$  photons with polarization  $\pi$  and  $m$  photons with polarization  $\pi_\perp$ . Subsequently, the dichotomization of the measurement corresponds to assign the value (+1) if  $n_\pi - m_{\pi_\perp} > k$ , (-1) if  $m_{\pi_\perp} - n_\pi > k$ , and (0) otherwise (Fig.2-(a)). This choice of the detection scheme corresponds to the POVM operators:

$$\hat{F}_{\pi, \pi_\perp}^{(+1)}(k) = \sum_{n=k}^{\infty} \sum_{m=0}^{n-k} \hat{\Pi}_{n,m} \quad (3)$$

$$\hat{F}_{\pi, \pi_\perp}^{(-1)}(k) = \sum_{m=k}^{\infty} \sum_{n=0}^{m-k} \hat{\Pi}_{n,m} \quad (4)$$

$$\hat{F}_{\pi, \pi_\perp}^{(0)}(k) = \hat{I} - \hat{F}_{\pi, \pi_\perp}^{(+1)} - \hat{F}_{\pi, \pi_\perp}^{(-1)} \quad (5)$$

The discarded outcome (gray (0) region in Fig.2-(a)) turns out to be state dependent. This property, as we shall see later, renders this kind of dichotomic measurement not fair for applications in Bell's inequalities test.

### B. Threshold detection

We now introduce a different dichotomic measurement method which is based on a threshold detection scheme. Let us consider the following apparatus. As in the OF case, the incident field is analyzed in polarization on each spatial mode by photon-counting detectors, and the Von Neumann operators that describe this intensity measurement are again the  $\hat{\Pi}_{n,m}$  projectors. The dichotomization of the measurement then proceeds as follows (Fig. 2-(b)). The (+1) outcome is assigned when the threshold condition  $n_\pi + m_{\pi_\perp} > h$  is satisfied and when  $n_\pi > m_{\pi_\perp}$ . Analogously, the (-1) outcome is assigned in the opposite case  $n_\pi < m_{\pi_\perp}$  conditionally to the threshold condition:  $n_\pi + m_{\pi_\perp} > h$ . If  $n_\pi = m_{\pi_\perp}$ , one of the two outputs ( $\pm 1$ ) is randomly assigned with equal probability  $p = 1/2$ . The POVM operators that describe the

measurement can then be written in the form:

$$\hat{T}_{\pi, \pi_\perp}^{(+1)}(h) = \sum_{n=h}^{\infty} \sum_{m < \frac{n}{2}} \hat{\Pi}_{n-m, m} \quad (6)$$

$$\hat{T}_{\pi, \pi_\perp}^{(-1)}(h) = \sum_{n=h}^{\infty} \sum_{m > \frac{n}{2}} \hat{\Pi}_{n-m, m} \quad (7)$$

$$\hat{T}_{\pi, \pi_\perp}^{(0)}(h) = \hat{I} - \hat{T}_{\pi, \pi_\perp}^{(+1)} - \hat{T}_{\pi, \pi_\perp}^{(-1)} \quad (8)$$

This scheme has the peculiar property of selecting an invariant region of the Fock space with respect to rotations of the polarization basis. More specifically, let us consider the case in which the measurement is performed choosing a polarization basis  $\pi, \pi_\perp$ . With that choice, all the pulses for which  $n_\pi + m_{\pi_\perp} \leq h$  are not detected. Rotating the basis to  $\pi', \pi'_\perp$ , the undetected part of the wave function still corresponds to the application of the same threshold condition in the new basis  $n_{\pi'} + m_{\pi'_\perp} > h$ . Hence, the filtered Fock-space region is independent on the choice of the polarization basis but is a function only of the threshold  $h$ , which is an intrinsic property of the detection apparatus. This feature is the main difference with the OF device discussed in previous section, and renders the TD based detection strategy feasible for its implementation in Bell's inequalities tests.

## IV. BELL'S INEQUALITIES BETWEEN MACROSCOPIC PHOTONIC STATES GENERATED BY HIGH GAIN SPONTANEOUS-PARAMETRIC DOWN-CONVERSION

In this section we perform a theoretical investigation on non-locality in a specific macroscopic quantum system analyzed with the threshold detection apparatus previously introduced. Specifically, we investigate the quantum correlations between the fields associated to modes  $\mathbf{k}_A$  and  $\mathbf{k}_B$  of the state of Eq.(1) by using the dichotomic measurements described in the previous section. More specifically, we derive the interference fringe pattern obtained by varying the polarization analysis basis on mode  $\mathbf{k}_B$ . As a first step, we consider individually the singlet spin- $\frac{\pi}{2}$  states (2), and we subsequently extend the results to the SPDC output superposition state of Eq. (1). To generalize the results to a realistic detection and transmission apparatus, we numerically simulate the effect of losses and non-unitary detection efficiency in the interference fringe pattern. Finally, we address the problem of non-locality by investigating a CHSH inequality for this detection apparatus, studying how the amount of violation is modified by the increase in the photon's number  $n$ .

### A. Interference fringe pattern on singlet spin- $\frac{n}{2}$ states

We begin our analysis on the macroscopic-macroscopic state by evaluating the correlations existing between the two spatial modes of the spin- $\frac{n}{2}$  singlet states (Eq.(2)). We use a pure dichotomic measurement scheme, where the (+1) and (-1) outcomes are assigned whether the difference in the number of photons with two orthogonal polarization is positive or negative. Finally, if the detected difference in the number of photons is 0, one of the ( $\pm 1$ ) outcomes is randomly assigned to the event with equal probability  $p = 1/2$ . We note that this choice is a sub-case of the threshold detection and O-filtering methods introduced in the previous Section, corresponding to the values  $h = 0$  and  $k = 0$ .

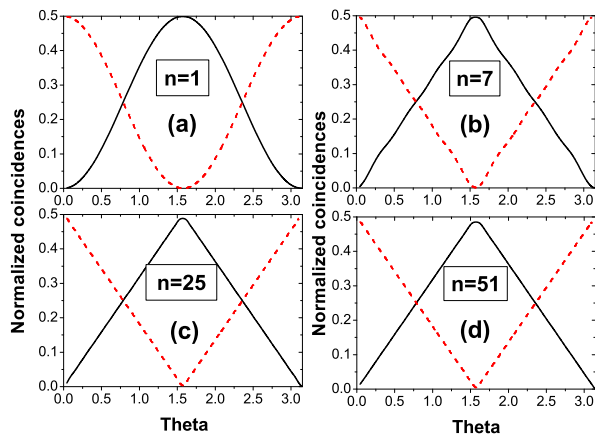


FIG. 3: (Color online) Theoretical interference fringe-patterns for singlet spin- $\frac{n}{2}$  states. The polarization basis on mode  $\mathbf{k}_A$  is kept fixed while on mode  $\mathbf{k}_B$  the basis is varied to obtain the fringe pattern. Figures correspond to values of (a)  $n = 1$ , (b)  $n = 7$ , (c)  $n = 25$  and (d)  $n = 51$ . The sinusoidal pattern of the spin- $\frac{1}{2}$  progressively transforms into a linear pattern. In all figures, black continuous line corresponds to the coincidences of both the (+1,+1) and (-1,-1) outcome configurations, while red dashed line corresponds to the (+1,-1) and (-1,+1) outcomes on the two spatial mode. Note that the maximum for each fringe is 0.5, which is the probability to obtain one of the two possible anti-correlated outcomes ( $\mp 1, \pm 1$ ).

The scheme for evaluating the correlations is sketched in Fig. 1. The two spatial modes of the  $|\psi_n^-\rangle$  are analyzed with the dichotomic measurement apparatus here described. The polarization's basis on mode  $\mathbf{k}_A$  is fixed on  $\{\vec{\pi}_+, \vec{\pi}_-\}$ , while on mode  $\mathbf{k}_B$  the analysis basis is varied over the Bloch sphere. In particular, due to the SU(2) symmetry of the emitted states, it is sufficient to consider only the linear polarizations case, defined by the rotation:  $\vec{\pi}_\theta = \cos \theta \vec{\pi}_+ + \sin \theta \vec{\pi}_-$ . The fringe patterns are then obtained by evaluating the coincidences between

the outcomes of the two detection apparatus on modes  $\mathbf{k}_A$  and  $\mathbf{k}_B$ . More specifically, this measurement corresponds to the evaluation of the averages:

$$\begin{aligned} D_{|\psi_n^-\rangle}^{(\pm 1, \pm 1)}(\theta) &= \langle \psi_n^- | \left( \hat{T}_{+,-}^{(\pm 1)}(0) \right)_A \otimes \left( \hat{T}_{\theta, \theta_\perp}^{(\pm 1)}(0) \right)_B | \psi_n^- \rangle \\ &= \langle \psi_n^- | \left( \hat{F}_{+,-}^{(\pm 1)}(0) \right)_A \otimes \left( \hat{F}_{\theta, \theta_\perp}^{(\pm 1)}(0) \right)_B | \psi_n^- \rangle \end{aligned} \quad (9)$$

The calculation of this measurement has been analytically performed by expressing the singlet spin- $\frac{n}{2}$  states of eq.(2) in the analyzed polarization basis:

$$|\psi_n^-\rangle = \sum_{m=0}^n \sum_{p=0}^n \epsilon_{m,p}^n(\theta) |(n-m)_+, m-\rangle_A |p\theta, (n-p)\theta_\perp\rangle_B \quad (10)$$

where:

$$\begin{aligned} \epsilon_{m,p}^n(\theta) &= \sum_{q(m,p)} (-1)^q \alpha_\theta^{m+p-2q} \beta_\theta^{n-m-p+2q} \\ & \quad [C_{p-q}^{n-m} C_{m-q}^{n-p} C_q^m C_q^p]^{\frac{1}{2}} \end{aligned} \quad (11)$$

with  $\alpha_\theta = \cos \theta$ ,  $\beta_\theta = \sin \theta$  and  $C_j^i = \frac{i!}{j!(i-j)!}$  is the binomial coefficient. The limits of the sum over  $q$  have an explicit dependence on the values of  $p$  and  $m$  and are not reported here. Finally, by direct application of the measurement operator, the interference fringe patterns are evaluated as:

$$D_{|\psi_n^-\rangle}^{(\pm 1, \pm 1)}(\theta) = \sum_{\{m,p\}} |\epsilon_{m,p}^n(\theta)|^2 \quad (12)$$

The extension of the sums over  $m$  and  $p$  depends on the choice of the outcome on each spatial mode according to the definitions of Eqs.(3-5) and (6-8).

In Fig.3 we report the results obtained for different values of the number of photons  $n$ . The simplest case, corresponding to a spin- $\frac{1}{2}$  state, presents the well-known sinusoidal pattern, as shown in Fig. 3-(a). The sinusoidal pattern is responsible for the violation of Bell's inequalities as no classical system can present this dependence from the phase  $\theta$ . For progressively higher values of  $n$ , as shown in Fig. 3-(b-d), the fringe pattern changes its dependence from the phase from a sinusoidal to a linear form. The latter represents the typical response of a pair of classically anti-correlated spin- $\mathbf{J}$  systems, analyzed through a dichotomic "which emisphere" measurement [29, 30], i.e. the measurement of the angular momentum sign. Such detection scheme is completely analogous to the dichotomic strategy analyzed in this section.

The transition with increasing  $n$  towards a classical response for the singlet spin- $\frac{n}{2}$  can be explained observing that the chosen dichotomic detection scheme is no more sufficient to fully characterize the singlet spin states of increasing size  $n > 1$ . This measurement lacks of the necessary resolution [31] to observe the peculiar quantum properties of these states. In other words, this measurement scheme is not sufficient to fully extract the

information encoded in the polarization anti-correlation of the singlet spin states. Their characterization would require a more sophisticated detection apparatus able to discriminate the value  $m$  of the spin projection, i.e. in our case the difference in the orthogonally polarized photon number, and not only its sign. An example of such measurement [9] is given by the parity operator  $\hat{P}_{\pi, \pi_{\perp}} = \sum_{m=0}^n (-1)^m |(n-m)\pi, m\pi_{\perp}\rangle \langle (n-m)\pi, m\pi_{\perp}|$ .

The correlation between the two spatial modes of the singlet spin- $\frac{n}{2}$  states evaluated with this measurement operator leads to the following expression:

$$\begin{aligned} P_{|\psi_n^-\rangle}(\theta) &= \langle \psi_n^- | \left( \hat{P}_{+, -} \right)_A \otimes \left( \hat{P}_{\theta, \theta_{\perp}} \right)_B | \psi_n^- \rangle \\ &= (-1)^n \frac{\sin[(n+1)\theta]}{(n+1) \sin \theta} \end{aligned} \quad (13)$$

This correlation function violates a CHSH inequality of an amount  $S_{CHSH} = 2.481 > 2$  [9] even in the asymptotic limit of large number of particle ( $n \rightarrow \infty$ ). However, such scheme based on the parity operator requires a sharp photon number measurement in order to discriminate with unitary efficiency among contiguous values of the spin projection.

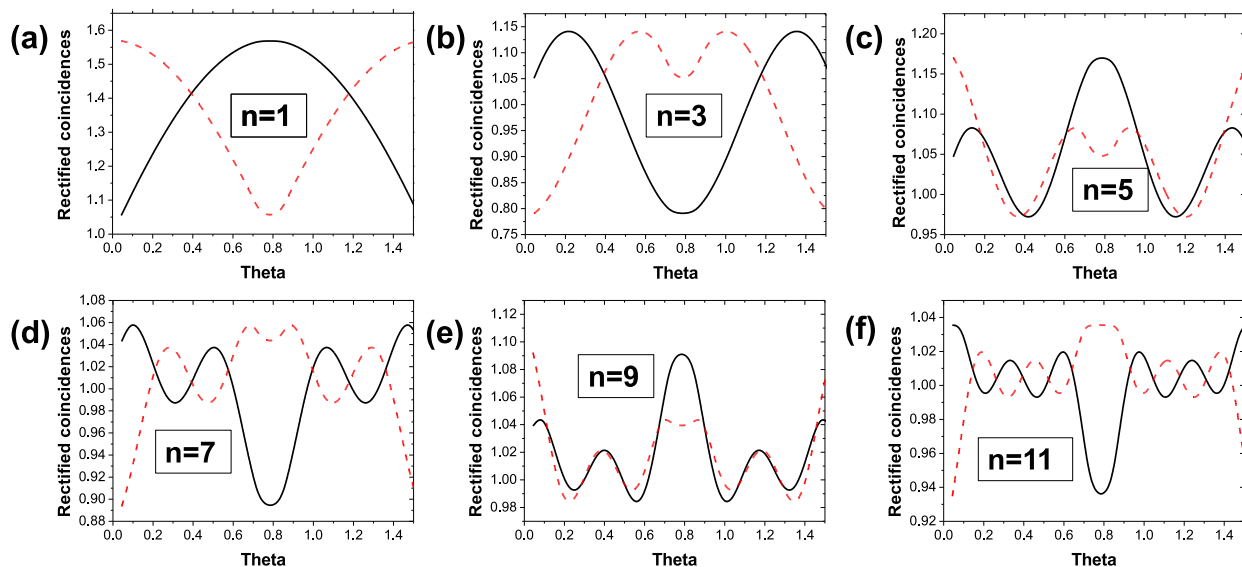


FIG. 4: (Color online) Plot of the interference fringe pattern  $D_{|\psi_n^-\rangle}^{(\pm 1, \pm 1)}(\theta)$  for singlet spin- $\frac{n}{2}$  states divided by a linear function  $L(\theta)$  corresponding to the behaviour of two distinct classical macroscopic objects. Black continuous lines corresponds to the coincidences of both the  $(+1, +1)$  and  $(-1, -1)$  outcome configurations, while red dashed lines correspond to the  $(+1, -1)$  and  $(-1, +1)$  outcomes on the two spatial mode.

As a further analysis, let us plot (Fig.4) the function  $D_{|\psi_n^-\rangle}^{(\pm 1, \pm 1)}(\theta)/L(\theta)$ , which corresponds to the ratio between the interference fringe pattern of the macro-macro configuration and a linear function of  $\theta$ . The choice of the curve  $L(\theta)$  as a reference is motivated by the following consideration. The evaluation of the CHSH parameter in a system characterized by the linear response leads to the maximum value in a classical framework  $S_{CHSH} = 2$ . Hence, this function  $L(\theta)$  can be considered as the boundary between the “classical” and the “quantum” regions, since it represents the response of

two classical anti-correlated systems to this test. In Fig.4, we note that the ratio  $D_{|\psi_n^-\rangle}^{(\pm 1, \pm 1)}(\theta)/L(\theta)$  presents a number of intersections with the axis  $y = 1$  (unitary ratio) proportional to the value of  $n$ . This depends on the explicit functional form of the interference fringe pattern of Eq.(12). Indeed, analyzing the explicit expression (Eq.(11)) of the coefficients  $\epsilon_{m,p}^n(\theta)$ , we find a sum of terms  $(\cos \theta)^{m+p-2q} (\sin \theta)^{n-m-p+2q}$ , where the sum of the exponents is equal to the number of photons  $n$ . Hence, the fringe pattern  $D_{|\psi_n^-\rangle}^{(\pm 1, \pm 1)}(\theta)$  (Eq.(12)) can be re-organized in a Fourier series expansion containing all

the Harmonics up to  $k = 2n$ . With increasing  $n$ , the difference between  $D_{|\psi_{\pm}^n\rangle}^{(\pm 1, \pm 1)}(\theta)$  and the linear function  $L(\theta)$  is progressively reduced, since more harmonics are present in the Fourier expansion which asymptotically reaches the expansion of  $L(\theta)$ .

In conclusion, the increase in the number of photons renders the dichotomic measurement inefficient for the complete characterization of the state, and the decreased correlations become more similar to classical ones.

## B. Propagation over a lossy channel

Decoherence in macroscopic systems represents the main cause for the impossibility of observing quantum phenomena in every-day life and for the realization of quantum experimental schemes. In the previous section we described a correlation experiment based on dichotomic detection in an ideal setup, where both the transmission channel and the detection apparatus possess unitary quantum efficiency. However, in real setups loss in both stages must be considered. Hence, the investigation on the effects of decoherence allows to understand both the transition from the quantum to the classical world and the feasibility of the schemes here presented in order to violate the Bell's inequalities.

To this end, we introduce a beam-splitter model [32, 33] to simulate losses phenomena on the macroscopic field here analyzed. In particular, the analysis has been performed for any singlet spin- $\frac{n}{2}$  state which, in the decoherence-free case, exhibits the transition from a sinusoidal interference pattern ( $n = 1$ ) to an asymptotic linear interference fringe pattern ( $n \gg 1$ ). Again, the detection scheme used is a pure dichotomic measurement apparatus (corresponding to the threshold detector and a O-Filter with  $h = k = 0$ ). As the measurement operators of Eqs. (3-8) are linear combination of Fock-state projectors, the lossy channel can be simulated numerically. More specifically, our calculation is divided in the following steps. First, for a set of angles  $\theta$  of the analysis basis on spatial mode  $\mathbf{k}_B$ , we calculated the coefficients of the state  $\epsilon_{m,p}^n(\theta)$  defined in Eq.(11). As the measurement operators are diagonal in the Fock basis, the results of the measurement depend only on the diagonal part of the density matrix after losses. Furthermore, the map that describes the lossy process, i.e.  $\mathcal{L}[\hat{\rho}] = \sum_k \gamma_k \hat{a}^k \hat{\rho} \hat{a}^{\dagger k} \gamma_k^\dagger$  where  $\gamma_k = \frac{1}{\sqrt{k!}}(1 - \eta)^{k/2} \eta^{(\hat{a}^\dagger \hat{a})/2}$ , maps diagonal elements in diagonal elements of the density matrix. All these considerations allow us to focus our numerical analysis on the diagonal part of the density matrix. The numerical simulation proceeds as follows. Let us for example focus our attention on the  $(+1, +1)$  joint outcome. The coefficients of the distribution  $|\epsilon_{m,p}^n(\theta)|^2$  are arranged in a matrix form, labelled by the row and column indexes  $(m, p)$ . For each value of  $m$  and  $p$ , 4 binomial random number generators with average values respectively  $\{(n - m)\eta, m\eta, p\eta, (n - p)\eta\}$  simulate a single shot

passage of the  $|(n - m)+, m-\rangle_A \otimes |p\theta, (n - p)\theta_\perp\rangle_B$  element through the lossy channel of efficiency  $\eta$ . Then, the output number of photons transmitted by the channel on each spatial mode are dichotomically compared, assigning 1 to the event if it belongs to the  $(+1, +1)$  joint outcome configuration and 0 otherwise. We then repeat this procedure  $N$  times, averaging the results of the simulation for each value  $m$  and  $p$ , thus generating a matrix  $M_{m,p}^{(+1, +1)}$  containing both the transmission and the measurement processes. Finally, the point  $D_{\hat{\rho}_{n,\eta}}^{(+1, +1)}(\theta)$  is reconstructed combining the matrix  $M_{m,p}^{(+1, +1)}$  that describes the dynamical process and the original photon number distribution of the state in the chosen basis, according to:

$$D_{\hat{\rho}_{n,\eta}}^{(+1, +1)}(\theta) = \sum_{m,p=0}^n M_{m,p}^{(+1, +1)} |\epsilon_{m,p}^n(\theta)|^2 \quad (14)$$

The same procedure is applied for the other three outcomes of the joint dichotomic measurements. The results of the simulation for different values of the channel transmittivity  $\eta$  are reported for a fixed value of  $n = 51$  in Fig.5. As the efficiencies of the channel and the detection scheme decrease, the linear fringe patterns progressively evolve into sinusoidal ones, at the cost of a smaller value of the visibility.

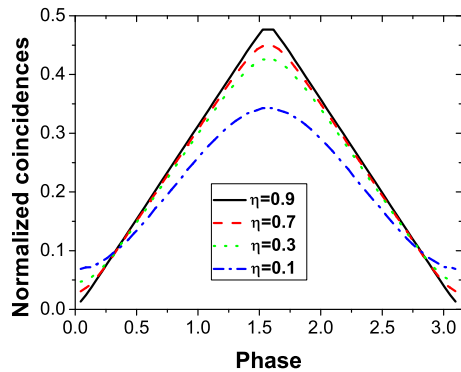


FIG. 5: (Color online) Interference fringe pattern in presence of losses for the singlet spin- $\frac{n}{2}$  state for  $n = 51$ . The effect of the lossy channel is the progressive lowering of the visibility, while the dependence on the phase changes from a linear to a sinusoidal pattern.

## C. O-Filtering and Threshold detection in a lossy regime

The analysis performed on the correlations present in the singlet spin- $\frac{n}{2}$  states has been focused on the detection by a pure dichotomic scheme. We are now interested in observing the effects of more sophisticated

POVM measurements, as the threshold detection or the O-filtering methods introduced in Section III. In particular, we analyze how both the visibility and the form of the fringe pattern are modified exploiting this different measurement schemes. The main idea beyond this approach concerns the possibility of beating the losses effects on the macro-macro correlations, by using a more sophisticated measurement than a pure dichotomic one.

We first analyze the correlations obtained by the O-Filtering detection scheme, introduced in Section III A. The fringe pattern can be calculated by evaluating the average:

$$F_{|\psi_{\bar{n}}\rangle}^{(\pm 1, \pm 1)}(\theta, h) = \left\langle \left( \hat{F}_{+,-}^{(\pm 1)}(h) \right)_A \otimes \left( \hat{F}_{\theta, \theta_{\perp}}^{(\pm 1)}(h) \right)_B \right\rangle \quad (15)$$

We performed a numerical simulation, in order to consider also the transmission over a lossy channel, with a procedure analogous to the one described in the previous section. We report in Fig.6 the fringe pattern obtained for the  $n = 51$  singlet states for two values of the channel efficiency. We note that, as the OF threshold  $k$  is increased, the tails of the fringe pattern are damped, while the form of the fringe around the peaks remains unchanged. Furthermore, both the minimum and the maximum of the fringes are lowered by this filtering procedure. To understand the advantage of this measurement scheme with respect to the pure dichotomic case, we analyze in Fig.8 the trend of visibility of the fringe pattern as a function of the threshold. We note that, for increasing  $k$ , the visibility is increased by the filtering process. This advantage obtained by exploiting the O-filtering measurement can be explained by the following considerations. In absence of losses, the visibility of the fringe pattern is always unitary, as the analyzed state presents perfect polarization anti-correlations. After the transmission over a lossy channel, the binomial statistics added to the photon number distribution is responsible for the partial cancellation of this property. More precisely, if the difference between  $n_{\pi}$  and  $m_{\pi_{\perp}}$  on any of the two spatial mode is little, losses may invert the outcome of a dichotomic measurement, i.e. for example the (+1) outcome may be converted to the (-1) outcome if unbalanced losses occur in that specific event. Such a process can generate the occurrence in the joint measurement of a result with positive correlations, i.e. (+1,+1) or (-1,-1), where in the decoherence-free case only anti-correlations are present. Thus, the visibility of the fringe pattern can be reduced by the presence of losses. However, to invert the outcome of matrix elements with  $n_{\pi} - m_{\pi_{\perp}} = q \gg 0$ , a strongly unbalanced losses in a single shot for the two polarization modes must occur. This event has a decreasing probability as the difference  $q$  becomes larger. Since the O-filter device selects these zones of the Fock space which present such unbalancement, the outcome inversion becomes practically negligible and the visibility of the fringe pattern progressively returns unitary as the threshold  $k$  is increased.

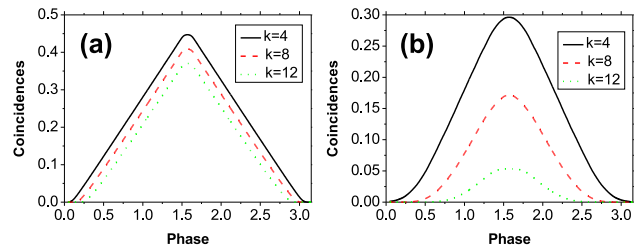


FIG. 6: (Color online) Effect of the O-Filtering detection technique on the fringe pattern of a  $n = 51$  singlet state. (a) Transmittivity  $\eta = 1$  and (b) transmittivity  $\eta = 0.3$ . As the threshold  $k$  is increased, the tails of the fringe pattern are rounded.

Let us now consider the second POVM dichotomic measurement under investigation, the threshold detection TD. The interference fringe pattern with this measurement scheme can be calculated as:

$$T_{|\psi_{\bar{n}}\rangle}^{(\pm 1, \pm 1)}(\theta, k) = \left\langle \left( \hat{T}_{+,-}^{(\pm 1)}(k) \right)_A \otimes \left( \hat{T}_{\theta, \theta_{\perp}}^{(\pm 1)}(k) \right)_B \right\rangle \quad (16)$$

In this expression, as before, the average is evaluated over the density matrix of the state after the numerical simulation of the lossy channel. In Fig.7 we report the form of the fringe pattern for  $n = 51$  and two different values of the transmittivity of the channel. As the threshold  $h$  is increased, we note that the TD device is responsible for the progressive return of the fringe patterns to their original form in absence of losses, i.e. for high values of  $n$  an approximately linear form. This behaviour can be explained as follows. While the original singlet-state has a well definite number of photons, the lossy channel reduces the number of photons to an average of  $\eta\langle n \rangle$ , with Poissonian fluctuations. At the measurement stage the threshold  $h$  in the TD device neglects (Fig.2-(b)) the sectors of the Fock-space corresponding to a low number of photons. As  $h$  approaches the value  $h = n$ , only the events in which the original singlet state travels undisturbed in the channel (with probability  $\eta^{2n}$ ) are selected, thus restoring the original correlation. We then analyze the effects of this measurement scheme in the visibility of the fringe pattern in Fig.8. We note that this quantity increases with a slower rate with respect to the OF apparatus. Differently from the O-filtering case, on each spatial mode the zones of the Fock space in which  $n_{\pi} - m_{\pi_{\perp}}$  is small are not filtered out, and the increase in the visibility is then much slower with the threshold  $h$ . However, also with the TD apparatus the visibility reaches asymptotically the unitary value, since as said for a threshold  $h = n$  only the original singlet state, having unitary visibility, is detected.

The analysis carried in this section than shows that both the OF and the TD detection strategies can be used to enhance the fringe pattern visibility in lossy conditions for the singlet spin- $\frac{n}{2}$  states. A comparison between the two schemes shows the better enhancement achievable

with the OF device. In Sec.IV D, we shall discuss in details the feasibility of a CHSH test with such measurements.

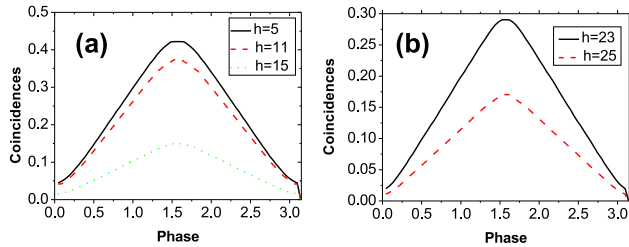


FIG. 7: (Color online) Effect of the Threshold detection technique on the fringe pattern for a  $n = 51$  singlet state. (a) Transmittivity  $\eta = 0.3$  and (b) transmittivity  $\eta = 0.5$ . As the threshold  $h$  on the total photon-number is increased, the fringe patterns progressively return to have approximately a linear dependence from the phase  $\theta$ , as for the original  $n = 51$  singlet state. The values of the thresholds are indicated in the figure.

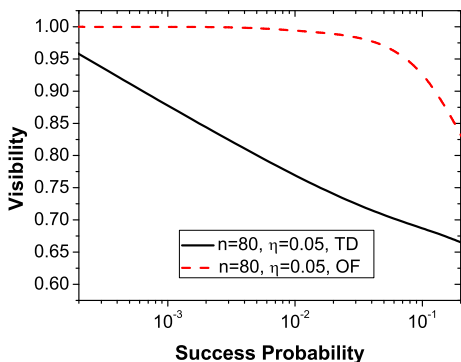


FIG. 8: (Color online) Trend of the visibility for the singlet spin states for  $n = 80$  and  $\eta = 0.05$ . The black straight curve corresponds to the TD detection scheme, while the red dashed line to the OF apparatus. In both cases, the success probability is calculated as the sum of the rate for the two conclusive outcomes (+1) and (-1).

#### D. Investigation of non-locality with a CHSH-type inequality

In the previous paragraphs of this Section we reported the interference fringe pattern obtained evaluating the correlations between singlet spin- $\frac{n}{2}$  states both in absence and in presence of experimental imperfections. The scheme here presented can be exploited to perform a CHSH test [2] to investigate non-local effects in these multiparticle states.

Let us briefly summarize in the light of a local hidden variable (LHV) theory the content of Bell inequalities for a set of dichotomic observables, by generalizing further the results already obtained by Reid *et al.* [16]. Consider a quantum state described by the density matrix  $\hat{\rho}$  defined in the Hilbert space  $\mathcal{H}_1 \otimes \mathcal{H}_2$ . Define  $\hat{O}_a^i$  the positive operator acting on subspace  $\mathcal{H}_1$ , and the probability of finding the value  $i$  after the measurement  $a$  as given by  $\text{Tr} [\hat{\rho}(\hat{O}_a^i \otimes \hat{I})]$ . The same relation holds for the positive operator  $\hat{O}_b^j$  acting on subspace  $\mathcal{H}_2$ .

The existence of a LHV model implies that the expectation values of the  $a$  and  $b$  are predetermined by the value of the parameter  $\lambda: \{X_a, X_{a'}, X_b, X_{b'}\}$ , hence the product  $a \cdot b$  is equal to  $X_a(\lambda)X_b(\lambda)$ . For a fixed value of  $\lambda$  the variables  $X_n$  with  $n = \{a, b, a', b'\}$  take the values  $-1, 1$  and satisfy the CHSH inequality:

$$X_a(\lambda)X_b(\lambda) + X_a(\lambda)X_{b'}(\lambda) + X_{a'}(\lambda)X_b(\lambda) - X_{a'}(\lambda)X_{b'}(\lambda) \leq 2 \quad (17)$$

The same inequality holds by integrating this equation on the space of the hidden variable ( $\lambda$ ):

$$\int_{\Omega} d\mathbb{P}(\lambda)X_a(\lambda)X_b(\lambda) + \int_{\Omega} d\mathbb{P}(\lambda)X_a(\lambda)X_{b'}(\lambda) + \int_{\Omega} d\mathbb{P}(\lambda)X_{a'}(\lambda)X_b(\lambda) - \int_{\Omega} d\mathbb{P}(\lambda)X_{a'}(\lambda)X_{b'}(\lambda) \leq 2 \quad (18)$$

where  $P(\lambda)$  is the measure of the  $\lambda$  probability space. If there is a local hidden variables model for quantum measurement taking values  $[-1, +1]$ , then the following inequality must be satisfied by the measured mean values:

$$S_{CHSH} = E^{\rho}(a, b) + E^{\rho}(a, b') + E^{\rho}(a', b) - E^{\rho}(a', b') \leq 2 \quad (19)$$

where  $E^{\rho}(a, b)$  can be expressed as a function of the LHV as  $E^{\rho}(a, b) = \int_{\Omega} X_a(\lambda)X_b(\lambda)d\mathbb{P}(\lambda)$ . The violation of (19) proves that a LHV variables model for the considered experiment is impossible.

In our case, the positive operators  $\hat{O}_{a(b)}^i$  are given by the dichotomic measurement operators  $\{\hat{T}_{\pi, \pi_{\perp}}^{(\pm 1)}(0), \hat{F}_{\pi, \pi_{\perp}}^{(\pm 1)}(0)\}$ . In order to theoretically investigate the feasibility of a CHSH test on the spin- $\frac{n}{2}$  states, we evaluated the  $S_{CHSH}$  parameter in such system. The value of the  $S_{CHSH}$  has been numerically maximized over the measurement angles  $\{\theta, \theta', \varphi, \varphi'\}$  of Alice's [ $\mathbf{a}(\theta)$  or  $\mathbf{a}'(\theta')$ ] and Bob's [ $\mathbf{b}(\varphi)$  or  $\mathbf{b}'(\varphi')$ ] the polarization basis. In Fig.9 we report the results obtained for different values of the number of photons, and hence the spin, of the analyzed state. We observe the decrease in the absolute value of  $S_{CHSH}^{|\psi_n\rangle}$  analogously to what reported in [16, 17] for an equivalent Bell's inequalities test. However, the asymptotic behavior for high  $n$  shows that the parameter  $S_{CHSH}$  never falls below the classical limit, but the amount of violation progressively becomes smaller and

any decoherence process may forbid its experimental observation.

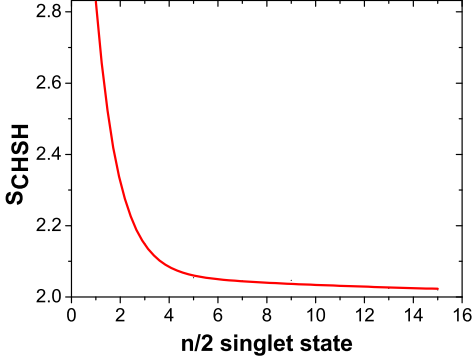


FIG. 9: (Color online) Value of the CHSH parameter  $S_{CHSH}^{|\psi_n^-\rangle}$  for singlet spin- $\frac{n}{2}$  states for an optimal choice of the angle settings and the dichotomic “majority-voting” measurement. We observe the progressive decrease in the amount of violation for an increasing value of the number of photons present in the state.

We now discuss the feasibility of a Bell’s inequality test when the OF and the TD detection methods are adopted in the context of Local Hidden Variables (LHV) models. This analysis is motivated by the increase in the visibility obtained with this measurement operators with respect to the pure dichotomic case. Both strategies present the POVM feature of having three possible outcomes  $\{-1, 1, 0\}$ , at variance with a genuine dichotomic measurement. In order to clarify the validity of a Bell test in presence of such kind of POVM’s, let us consider the case in which at the A site a standard dichotomic measurement is performed, while at the B site a POVM measurement is carried out.

Consider the outcomes for which the Bob’s results are different from 0. In this case the expectation value of the product of  $a$  and  $b$  is conditioned by the event: “outcome  $b$  different from zero”. In a LHV model these conditional expectations are represented by:

$$E^\rho(a \cdot b) = \int_{\Omega'} X_a(\lambda) X_b(\lambda) d\mathbb{P}'(\lambda) \quad (20)$$

where  $\Omega'$  is the hidden variable probability sub-space for which, for *any*  $X_{b'}(\lambda)$ , is  $X_b(\lambda) \neq 0$  and  $d\mathbb{P}' = d\mathbb{P} / \int_{\Omega'} d\mathbb{P}$ . Similarly:

$$E^\rho(a \cdot b') = \int_{\Omega''} X_a(\lambda) X_b(\lambda) d\mathbb{P}''(\lambda) \quad (21)$$

where  $\Omega''$  is the hidden variable probability sub-space for which, for *any*  $X_b(\lambda)$ , is  $X_{b'}(\lambda) \neq 0$  and  $d\mathbb{P}'' = d\mathbb{P} / \int_{\Omega''} d\mathbb{P}$ . Since for different random variables  $X_b$  and  $X_{b'}$  these conditional expectations values can in principle

refer to different subensembles  $\Omega'$  and  $\Omega''$  of the original ensemble  $\Omega$ , in general the equation (18) doesn’t hold any more and the measured quantity, based on the detection of conditional values, is:

$$\int_{\Omega'} d\mathbb{P}'(\lambda) X_a(\lambda) X_b(\lambda) + \int_{\Omega'} d\mathbb{P}'(\lambda) X_{a'}(\lambda) X_b(\lambda) + \int_{\Omega''} d\mathbb{P}''(\lambda) X_a(\lambda) X_{b'}(\lambda) - \int_{\Omega''} d\mathbb{P}''(\lambda) X_{a'}(\lambda) X_{b'}(\lambda) \quad (22)$$

Let us consider the class of LHV models such that, for a fixed value of  $\lambda$ , simultaneously is:  $X_b(\lambda) \neq 0, X_{b'}(\lambda) \neq 0$ . In this case the inequality (17) still holds since it becomes:

$$\int_{\Omega^*} d\mathbb{P}^*(\lambda) X_a(\lambda) X_b(\lambda) + \int_{\Omega^*} d\mathbb{P}^*(\lambda) X_a(\lambda) X_{b'}(\lambda) + \int_{\Omega^*} d\mathbb{P}^*(\lambda) X_{a'}(\lambda) X_b(\lambda) - \int_{\Omega^*} d\mathbb{P}^*(\lambda) X_{a'}(\lambda) X_{b'}(\lambda) \leq 2 \quad (23)$$

where  $\Omega^*$  is the hidden variable probability common sub-space for which  $X_b(\lambda) \neq 0$  and  $X_{b'}(\lambda) \neq 0$ .

With reference to our experimental situation, let us now make an auxiliary assumption implying that the probability of rejecting a measurement does not depend on the hidden parameter  $\lambda$  and on the measurement settings, i.e.  $\Omega' = \Omega'' = \Omega^*$  [34]. In this case the experimentally observed quantity (22) will follow the LHV inequality (23), and its violation implies the non-locality of the considered system. While for what concerns the OF based strategy this assumption on the LHV is a strong one, in the TD case it is legitimated by the fact that the Hilbert subspace leading to a conclusive outcome is invariant under any rotation of the polarization basis since data are excluded depending only on the overall number of photons. In other words, when an event leads to a  $(\pm 1)$  outcome for a specific choice of the measurement basis, it would correspond to a conclusive outcome if measured in another basis. This scenario is exactly the same encountered in any two-photon Bell inequality test and hence requires a fair sampling assumption.

To conclude the discussion, we briefly analyze the advantages of the two POVM schemes presented here in terms of the achievable violation of the CHSH inequality  $S_{CHSH} - 2$ . In the OF case, we expect that the fast increase in the visibility may lead to an increase in the amount of violation with respect to the pure dichotomic measurement. In the TD case, as already discussed in the previous section, the effect of the threshold  $h$  is the restoration of the original correlations present in the  $|\psi_n^-\rangle$  state before the lossy channel. This means that the value of the  $S_{CHSH}$  parameter reaches for  $h = n$  the maximum value  $S_{CHSH}^{|\psi_n^-\rangle}$ , reported in Fig.9, and the amount of achievable violation becomes practically negligible for large  $n$ .

### E. Spontaneous Parametric Down Conversion: interference fringe pattern

The following step of our theoretical analysis is the investigation on the interference fringe pattern obtained by the process of spontaneous parametric down conversion exploiting the dichotomic measurement schemes presented in Sec.III. As already stressed in Eqs.(1-2), this optical source generates a quantum superposition of the singlet spin- $\frac{n}{2}$  states. We performed the same calculation of Sec.IV C in order to analyze both the form of the interference fringe pattern and the trend of the visibility when the two dichotomic measurements (OF and TD) were exploited at the detection stage.

We then report in Fig.10 the form of the fringe pattern for the SPDC output state in presence of losses, with  $g = 2.5$  and  $\eta = 0.5$ . Analogously to what observed for singlet spin states, the effect of the two measurement devices is different. On one side, the O-filtering technique is responsible for a smoothing of the fringe pattern tails, while on the other side, the Threshold Detector leaves the form of the fringe pattern unaltered.

To conclude the analysis of this section, we report in Fig.11 the trend of the visibility of the fringe pattern as a function of the success probability of the two dichotomic measurement devices. A comparison between the technique shows the faster increase of the visibility in the OF case (Fig.11-(a)) with respect to the TD one (Fig.11-(b)). The cost of this faster increase in the visibility is a loss in the universality of the device, since the Threshold Detector selects a regions of the Fock space which is invariant under rotations of the polarization basis, at variance with the O-filter.

### V. EXPERIMENTAL OBSERVATION OF CORRELATIONS IN HIGH GAIN SPDC

In order to complete our analysis on the correlations connecting a macro-macro state obtained via high gain optical parametric amplification, we have experimentally investigated the conceptual scheme presented in the previous sections. We have generated a multiphoton state through an EPR source and we have performed dichotomic measurement via O-Filter (OF) and Threshold Detector (TD) upon it. In this section we report the experimental interference fringe patterns observed for the spontaneous field generated by the high gain OPA working in a non collinear configuration. As a first step we shall characterize the OPA in a high gain regime, by evaluating the non linear gain of the amplifier and by reporting the generated field fringe pattern visibility as a function of the gain. Then, we shall investigate the features of the multiphoton field through the two measurement strategies studied in Sec. III.

Let us now describe the experimental setup shown in Fig.12. The excitation source was a Ti:Sapphire Coherent Mira mode-locked laser amplified by a Ti:Sapphire

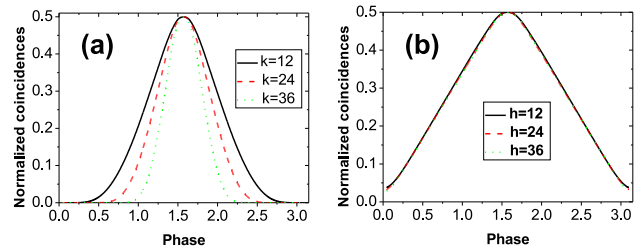


FIG. 10: (Color online) Fringe pattern in presence of losses for the SPDC output state with the two different analyzed dichotomic measurements. In all curves,  $g = 2.5$  and  $\eta = 0.5$ . (a) Normalized fringe pattern with the O-filter device for different values of the threshold  $k$ . The three curves correspond to a filtering signal of  $P(k = 12) = 0.116$  (black straight curve),  $P(k = 24) = 0.014$  (red dashed curve) and  $P(k = 36) = 2.07 \times 10^{-4}$  (green dotted curve). We note the increase in the smoothing of the minimum of the fringes. (b) Normalized fringe pattern with the TD device for different values of the threshold  $h$ . The three curves correspond to a filtered signal of  $P(h = 12) = 0.328$  (black straight curve),  $P(h = 24) = 0.068$  (red dashed curve) and  $P(h = 36) = 1.07 \times 10^{-3}$  (green dotted curve). We note that the form of the normalized fringes is left unchanged by the TD device.

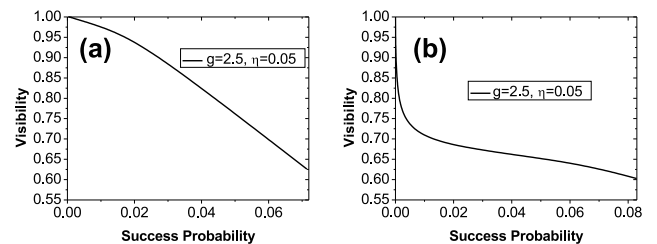


FIG. 11: (Color online) (a) Visibility of the fringe pattern as a function of the success probability  $\langle \hat{F}_{\pi, \pi_{\perp}}^{(+1)}(k) \rangle + \langle \hat{F}_{\pi, \pi_{\perp}}^{(-1)}(k) \rangle$  for the SPDC states analyzed with the OF device. (b) Visibility of the fringe pattern as a function of the success probability  $\langle \hat{T}_{\pi, \pi_{\perp}}^{(+1)}(h) \rangle + \langle \hat{T}_{\pi, \pi_{\perp}}^{(-1)}(h) \rangle$  for the SPDC states analyzed with the TD device. For both curves,  $g = 2.5$  and  $\eta = 0.05$ .

regenerative RegA device operating with repetition rate 250 kHz. The output beam, frequency-doubled by second-harmonic generation, provided the OPA excitation field beam at the UV wave-length (wl)  $\lambda = 397.5$  nm with power 600 mW on mode  $\mathbf{k}_P$ . The SPDC source was a BBO crystal cut for type-II phase-matching, working in a non-collinear configuration [21], in a high gain regime. The evaluated non linear gain is  $g = 3.49 \pm 0.05$  corresponding to the generation of an average number of photons per mode of  $\bar{n} \approx 270$  per pulse, corresponding to an overall average value of  $\langle n \rangle \approx 540$  on each spatial mode.

The multiphoton fields on modes  $\mathbf{k}_A$  and  $\mathbf{k}_B$  were filtered by 1.5 nm interferential filters (IF) and coupled by

single mode fibers. The signals were then attenuated, analyzed in polarization and detected by single photon

SPCM detectors (not shown in Fig.12).

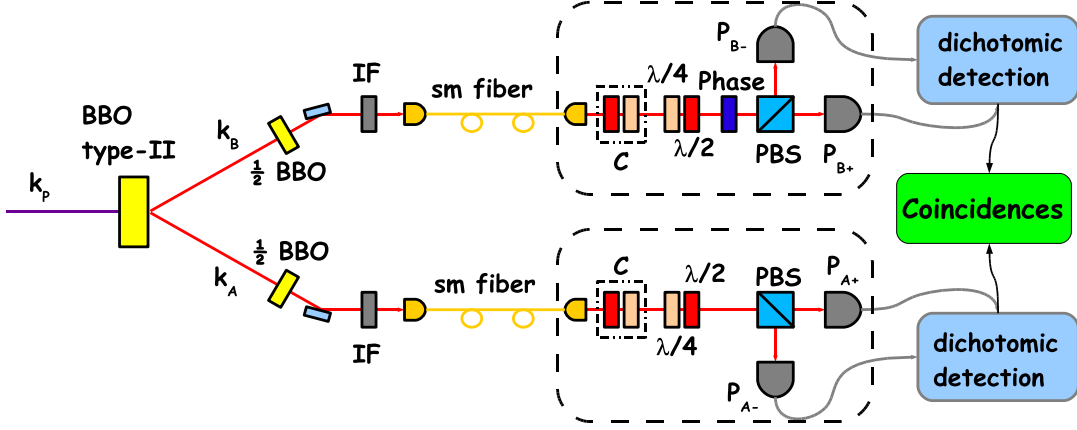


FIG. 12: (Color online) Experimental setup for the generation and detection of a bipartite macroscopic field. The high laser pulse on mode  $\mathbf{k}_P$  excites a type-II EPR source in the high gain regime, i.e.  $g = 3.5$ . The two spatial mode  $\mathbf{k}_A$  and  $\mathbf{k}_B$  are spectrally and spatially selected by interference filters (IF) and single mode fibers. After fiber compensation  $C$ , the two modes are analyzed in polarization and detected by four photomultipliers ( $P_{A+}, P_{A-}, P_{B+}, P_{B-}$ ). The signals are then analyzed electronically to perform either the threshold dichotomic detection described in the paper or the Orthogonality filtering detection technique. Finally, the coincidences between the measurement outcomes are recorded to obtain the desired interference fringe patterns.

In order to characterize the source, we performed a set of preliminary measurements exploiting a SPCM detector on both spatial modes, deliberately attenuating the generated in order to have only few photons incident on the detector. First, we measured the non-linear gain of the amplifier studying how the detected signal is increased by varying the power of the incident pump beam on the crystal. In Fig.13 we report the counts registered on mode  $\mathbf{k}_A$  by a SPCM detector as a function of the normalized UV power signal. The evaluation of the NL-gain has been performed as shown in Ref.[19], and, as said, we found  $g = 3.49 \pm 0.05$ . As a further investigation on the multiphoton field features, we registered the coincidences between the signals on mode  $\mathbf{k}_A$  and  $\mathbf{k}_B$ , as a function of the phase  $\varphi$ , that represents the variation of the polarization analysis basis on Bob site, i.e.  $\vec{\pi}_\varphi = \vec{\pi}_H + e^{i\varphi}\vec{\pi}_V$ . Both fields are detected by two SPCM at Alice's and Bob's sites. Again, the signals were attenuated in order to have few photons incident on the detectors, in order to work in a linear response regime for the SPCM. The visibility of the obtained fringe patterns as a function the NL-gain is shown in Fig. 14. As stressed in [19], the trend of visibility decreases as the gain increases, this is due to losses and to limited detectors photon number resolution. The decrease of visibility below the theoretical asymptotic value of 33% is due to the multimodal operation of the amplifier, although, differently from what is reported in [19], we observe a value

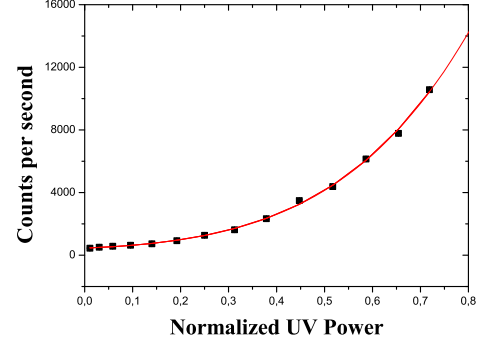


FIG. 13: (Color online) Experimental evaluation of the amplifier NL-gain: we report the counts of an SPCM detector on mode  $\mathbf{k}_A$  versus the normalized UV power, defined as  $I_{in}/I_{max}$ . The red curve reproduces the best fit of the experimental data, the expected trend function is reported in [19].

of visibility that remains above 15% as far as the NL-gain reaches the value of 3.5, while in [19] the visibility seems to fall below 15% for gain values higher than 2.

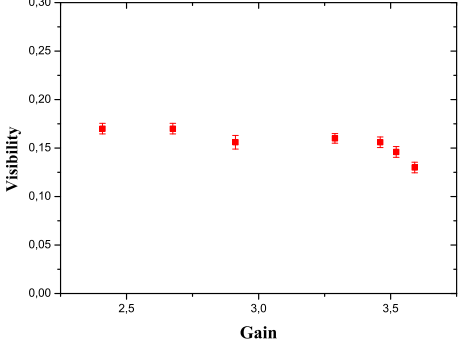


FIG. 14: (Color online) Experimental trend of the visibility as a function of the NL-gain.

### A. Non-collinear SPDC analyzed with the Orthogonality Filter

In this Section we report the observation of the fringe patterns obtained by the O-Filtering measurement strategy illustrated in Sec.III-A.

The multiphoton fields at Alice's and Bob's site are analyzed in polarization and detected by two photomultipliers (PMs),  $(P_{A+}, P_{A-})$  and  $(P_{B+}, P_{B-})$  respectively. This devices produce on each pulse a macroscopic output electronic current, whose amplitude is linearly proportional to the number of incident photons.

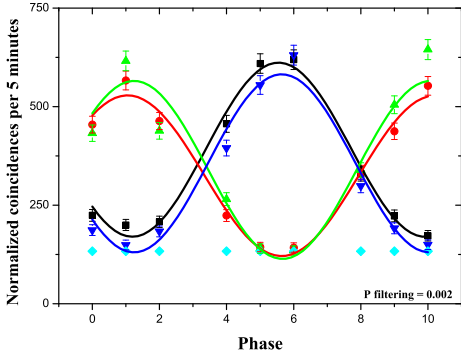


FIG. 15: (Color online) Fringe patterns obtained by filtering on the difference of the signals. The main visibility is  $0.67 \pm 0.02$ . Coincidences have been normalized to the product of the signals detected on each of the analyzed outcomes of the OF.

Let us fix the polarization analysis basis at Bob's site: the PMs provide the electronic signals  $(I_+^B, I_-^B)$  corresponding to the field intensity on the mode  $\mathbf{k}_B$  associated with the  $\pi$ -components  $(\vec{\pi}_+, \vec{\pi}_-)$ , respectively. By the OF, shot by shot the difference signals  $\pm(I_+^B - I_-^B)$  are compared with a threshold  $\xi k > 0$ , where  $\xi$  is a

constant describing the response of the photomultipliers. When the condition  $(I_+^B - I_-^B) > \xi k$  is satisfied, a standard transistor-transistor-logic (TTL) electronic square-pulse  $L_B$  is realized at one of the two output ports of OF. Likewise, when the condition  $(I_-^B - I_+^B) > \xi k$  is satisfied, a  $L_B^*$  TTL pulse is realized at other output port of OF. The PM output signals are discarded for  $-\xi k < (I_+^B - I_-^B) < \xi k$ , i.e. in condition of low state discrimination. By increasing the value of the threshold  $k$  an increasingly better discrimination is obtained together with a decrease of the rate of successful detection. The same measurement strategy is adopted at Alice's site, where the output TTL signals  $(L_A, L_A^*)$  are generated. The fringe patterns are obtained by the following procedure: the analysis basis at Alice's site is kept fixed while the basis at Bob's site is varied through an adjustable phase delay given by a Babinet-Soleil compensator. Finally the coincidences between the TTL signals at Alice's and Bob's site are taken into account, namely  $(L_A, L_B), (L_A, L_B^*), (L_A^*, L_B), (L_A^*, L_B^*)$ . We report in figure 15 the corresponding fringe patterns obtained in the  $\{\pi_+, \pi_-\}$  basis, analogous results are observed in the  $\{\pi_R, \pi_L\}$  and  $\{\pi_H, \pi_V\}$  basis, due to the irrotational invariance of the generated multiphoton state. The threshold  $k$  was set so that the percentage of data taken into account was  $2 \times 10^{-3}$  of the overall sample.

For sake of completeness we report the trend of visibility as a function of the OF counts in Fig.16. We observe an increase of visibility as the counts detected decrease. The highest visibility obtained is not enough to violate the CHSH inequality, due to the inefficiency of a dichotomic measurement performed on a multiphoton quantum state and to experimental imperfections. However, in accordance with theoretical predictions, we observe that the OF technique allows to minimize losses effects.

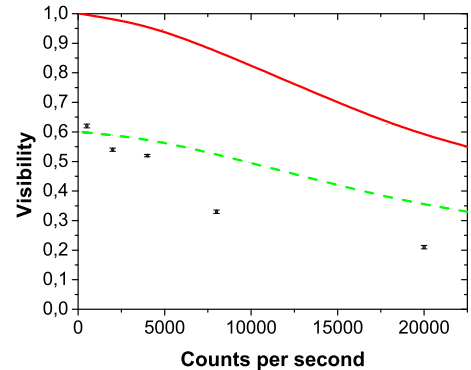


FIG. 16: (Color online) Trend of visibility versus OF counts. The theoretical predictions (continuous red line) has been renormalized (dotted green line) respect to the maximum reached visibility value.

## B. Non-collinear SPDC analyzed with threshold detection

A further investigation on the macro-macro correlation has been carried out by performing another dichotomic measurement on the amplified states on modes  $\mathbf{k}_A$  and  $\mathbf{k}_B$ . The signals detected by the photomultipliers ( $P_{A+}, P_{A-}$ ) and ( $P_{B+}, P_{B-}$ ) enter into two threshold detectors (TD), that performs the shot by shot measurement illustrated in Sec.III-B. Each TD works as follows: the PMs electronic signals ( $I_+^B, I_-^B$ ) ( $(I_+^A, I_-^A)$ ) corresponding to the field intensity on the mode  $\mathbf{k}_B$  ( $\mathbf{k}_A$ ), associated with the  $\pi$ -components ( $\vec{\pi}_+, \vec{\pi}_-$ ) respectively, enter into the TD. By it the sum signals  $\pm(I_+^B + I_-^B)$  ( $\pm(I_+^A + I_-^A)$ ) are compared with a threshold  $\xi h > 0$ . When the condition ( $I_+^B + I_-^B > \xi h$  and  $I_+^B - I_-^B > 0$ ) ( $(I_+^A + I_-^A > \xi h$  and  $I_+^A - I_-^A > 0)$ ) is satisfied, a standard transistor-transistor-logic (TTL) electronic square-pulse  $J_B$  ( $J_A$ ) is realized at one of the two output ports of TD. On the other hand when the condition ( $I_+^B + I_-^B > \xi h$  and  $I_-^B - I_+^B > 0$ ) ( $(I_+^A + I_-^A > \xi h$  and  $I_-^A - I_+^A > 0)$ ) is satisfied, a standard transistor-transistor-logic (TTL) electronic square-pulse  $J_B^*$  ( $J_A^*$ ) is realized at the other output ports of TD. Finally the coincidences between signals ( $J_A, J_B$ ), ( $J_A, J_B^*$ ), ( $J_A^*, J_B$ ), ( $J_A^*, J_B^*$ ) are registered by a coincidences box. The obtained fringe patterns corresponding to a detection probability equal to  $P = 1.6 \times 10^{-3}$  are shown in Fig.17. Finally, a study on the obtained visibility as a function of the fraction of considered data has been carried out. We report in Fig.18 the trend of visibility versus TDs counts.

## VI. CONCLUSION AND PERSPECTIVES

In this work we have reported a deep analysis on the possibility of observing quantum correlation on a multiphoton quantum system by performing probabilistic dichotomic measurements. We have addressed a specific

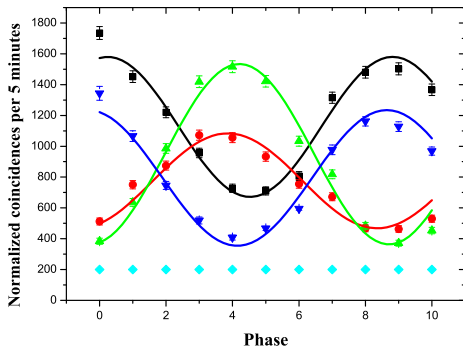


FIG. 17: (Color online) Fringe patterns obtained by filtering on the sum of the signals. The main visibility is  $0.49 \pm 0.02$ .

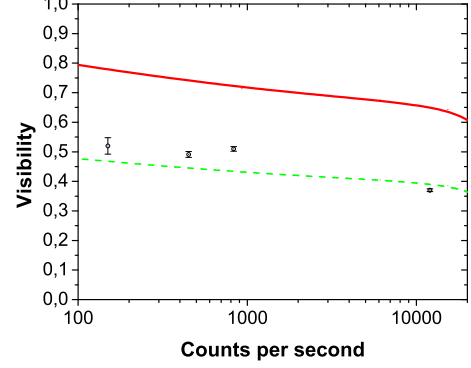


FIG. 18: (Color online) Visibility versus threshold detector counts. The theoretical predictions (continuous red line) has been renormalized (dotted green line) respect to the maximum reached visibility value.

class of multiphoton states: the ones obtained by the high gain optical parametric amplifier working in a non-collinear configuration. To this end we have introduced two kind of dichotomization processes, based on the O-Filtering procedure discussed in [27] and on a threshold detection scheme similar to the naked eye discussed in [35]. It has been demonstrated that these two detection schemes reduce to a simple dichotomic measurement when their characteristic thresholds are set to 0. We have shown that such dichotomic measurement when performed on  $\frac{n}{2}$ -spin states with increasing  $n$ , asymptotically allows in the ideal case the violation of CHSH Bell's inequality even for large  $n$ . The shape of correlation functions has been investigated, and we have shown that the sinusoidal correlation pattern, typical of an  $\frac{1}{2}$ -spin state, tends asymptotically to a triangular form, proper to classical correlations. When losses and decoherence are introduced the visibility of the correlation pattern is lowered and its shape turns out to be sinusoidal. In presence of losses, the violation of CHSH Bell's inequality is not allowed by a dichotomic measurement and more complicated detection schemes are required. We then discussed in terms of LHV models the feasibility of a CHSH test with the two probabilistic measurements presented in this paper.

Finally, we have shown experimentally that the measurement performed by the probabilistic dichotomic schemes, the O-Filter and the Threshold Detector, allow to obtain higher visibility of correlation functions, not enough to violate CHSH Bell's inequality, but effective to reduce losses and decoherence effects. An open question concerns the existence of entanglement criteria able to demonstrate the presence of entanglement in a "macro-macro" scenario, and the possibility of adopting the measurement devices introduced in this paper within such context.

In conclusion we believe that our analysis contributes

to shed light on the role of measurement performed on large size quantum systems, and on the possibility of

observing entanglement and quantum phenomena at a macroscopic level.

- 
- [1] J. Bell, *Physics* **1**, 195 (1964).
- [2] J. F. Clauser, M. A. Horne, A. Shimony, and R. A. Holt, *Phys. Rev. Lett.* **23**, 880 (1969).
- [3] Y. H. Shih, and C. O. Alley *Phys. Rev. Lett.* **61**, 2921 (1988).
- [4] Z. Y. Ou and L. Mandel *Phys. Rev. Lett.* **61**, 50 (1988).
- [5] T. E. Kiess, Y. H. Shih, A. V. Sergienko, and C. O. Alley *Phys. Rev. Lett.* **71**, 3893 (1993).
- [6] K. J. Resch, P. Walther, and A. Zeilinger *Phys. Rev. Lett.* **94**, 070402 (2005).
- [7] P. Walther, M. Aspelmeyer, K. J. Resch, and A. Zeilinger *Phys. Rev. Lett.* **95**, 020403 (2005).
- [8] W. H. Zurek, *Rev. Mod. Phys.* **75**, 715 (2003).
- [9] A. Peres, *Quantum Theory: Concepts and Methods* (Kluwer, 1993).
- [10] J. Kofler and C. Brukner, *Phys. Rev. Lett.* **99**, 180403 (2007).
- [11] J. Kofler and C. Brukner, *Phys. Rev. Lett.* **101**, 090403 (2008).
- [12] J. Kofler, N. Buric, and C. Brukner, arXiv.org:0906.4465 (2009).
- [13] H. Jeong, M. Paternostro, and T.C. Ralph, *Phys. Rev. Lett.* **102**, 060403 (2009).
- [14] Z.B. Chen, J.W. Pan, G. Hou, and Y.D. Zhang, *Phys. Rev. Lett.* **88**, 040406 (2002).
- [15] S. Portolan, O. Di Stefano, S. Savasta, F. Rossi, and R. Girlanda, *Phys. Rev. A* **73**, 020101(R) (2006).
- [16] M. D. Reid, W. J. Munro, and F. De Martini, *Phys. Rev. A* **66**, 033801 (2002).
- [17] J. D. Bancal, C. Branciard, N. Brunner, N. Gisin, S. Popescu, and C. Simon *Phys. Rev. A* **78**, 062110 (2008).
- [18] C. Simon, and D. Bouwmeester *Phys. Rev. Lett.* **91**, 053601 (2003).
- [19] H. S. Eisenberg, G. H. Khoury, G. A. Durkin, C. Simon, and D. Bouwmeester, *Phys. Rev. Lett.* **93**, 193901 (2004).
- [20] M. Caminati, F. De Martini, R. Perris, F. Sciarrino, and V. Secondi, *Phys. Rev. A* **73**, 032312 (2006).
- [21] P. G. Kwiat, K. Mattle, H. Weinfurter, A. Zeilinger, A. V. Sergienko, and Y. Shih *Phys. Rev. Lett.* **75**, 4337 (1995).
- [22] W.P. Grice and I.A. Walmsley *Phys. Rev. A* **56**, 1627 (1997)
- [23] M. Eibl, S. Gaertner, M. Bourennane, C. Kurtsiefer, M. Zukowski, and H. Weinfurter *Phys. Rev. Lett.* **90**, 200403 (2003).
- [24] H. Weinfurter and M. Zukowski, *Phys. Rev. A* **64**, 010102(R) (2001).
- [25] W. Wieczorek, C. Schmid, N. Kiesel, R. Pohlner, O. Gühne, and H. Weinfurter *Phys. Rev. Lett.* **101**, 010503 (2008).
- [26] E. Nagali, T. De Angelis, F. Sciarrino, and F. De Martini, *Phys. Rev. A* **76**, 042126 (2007).
- [27] F. De Martini, F. Sciarrino, and C. Vitelli, *Phys. Rev. Lett.* **100**, 253601 (2008).
- [28] P. Sekatski, N. Brunner, C. Branciard, N. Gisin, and C. Simon, *Phys. Rev. Lett.* **103**, 113601 (2009).
- [29] M. Redhead, *Incompleteness, Nonlocality, and Realism* (Oxford University Press, 1989).
- [30] N.V. Evdokimov, D.N. Klyshko, V.P. Komolov, and V.A. Yarochkin, *Phys. Usp.* **39**, 83 (1996).
- [31] F. Costa, N. Harrigan, T. Rudolph, and C. Brukner, arXiv.org:0902.0935v1 (2009).
- [32] R. Loudon, *The Quantum Theory of Light* (Oxford University Press, 2000).
- [33] U. Leonhardt, *Phys. Rev. A* **48**, 3265 (1993).
- [34] G. Adenier and A. Khrennikov, arXiv:quant-ph/0306045 (2003).
- [35] N. Brunner, C. Branciard, and N. Gisin, *Phys. Rev. A* **78**, 052110 (2008).